


Article

A Reduced GO-Graphene Hybrid Gas Sensor for Ultra-Low Concentration Ammonia Detection

Chang Wang ^{1,2} , Shaochong Lei ¹, Xin Li ^{1,2,*}, Shixi Guo ¹, Ping Cui ¹, Xianqi Wei ^{1,3}, Weihua Liu ^{1,2} and Hongzhong Liu ⁴

¹ Department of Microelectronics, School of Electronics and Information Engineering, Xi'an Jiaotong University, Xi'an 710049, China; wangc254@163.com (C.W.); leisc@mail.xjtu.edu.cn (S.L.); guoshixi@stu.xjtu.edu.cn (S.G.); cuiping_dc@163.com (P.C.); wei.wxq@163.com (X.W.); lwhua@mail.xjtu.edu.cn (W.L.)

² Guangdong Shunde Xi'an Jiaotong University Academy, Foshan 528300, China

³ Research Institute of Xi'an Jiaotong University, Hangzhou 311215, China

⁴ State Key Laboratory for Manufacturing Systems Engineering, Xi'an Jiaotong University, Xi'an 710049, China; hzliu@mail.xjtu.edu.cn

* Correspondence: lx@mail.xjtu.edu.cn; Tel.: +86-29-8266-3343

Received: 17 August 2018; Accepted: 14 September 2018; Published: 18 September 2018



Abstract: A hybrid structure gas sensor of reduced graphene oxide (RGO) decorated graphene (RGO-Gr) is designed for ultra-low concentration ammonia detection. The resistance value of the RGO-Gr hybrid is the indicator of the ammonia concentration and controlled by effective charge transport from RGO to graphene after ammonia molecule adsorption. In this hybrid material, RGO is the adsorbing layer to catch ammonia molecules and graphene is the conductive layer to effectively enhance charge/electron transport. Compared to a RGO gas sensor, the signal-to-noise ratio (SNR) of the RGO-Gr is increased from 22 to 1008. Meanwhile, the response of the RGO-Gr gas sensor is better than that of either a pristine graphene or RGO gas sensor. It is found that the RGO reduction time is related to the content of functional groups that directly reflect on the gas sensing properties of the sensor. The RGO-Gr gas sensor with 10 min reduction time has the best gas sensing properties in this type of sensor. The highest sensitivity is 2.88% towards 0.5 ppm, and the ammonia gas detection limit is calculated to be 36 ppb.

Keywords: graphene; reduced graphene oxide (RGO); sensitivity; signal-to-noise (SNR); gas sensor; detection limit

1. Introduction

Ammonia gas is widely present in the surrounding environment. It is a colorless, irritating odor and highly toxic gas, therefore, the detection of ammonia is very important due to the potential threat to people's health posed by ammonia [1,2]. Meanwhile, since ammonia is a byproduct of protein metabolism, the detection of ammonia can help clinicians assess diseases and state of health [3,4]. Due to the merits of non-invasion, quickness, convenience, and repeatability, exhaled ammonia detection has attracted more attention for early diagnosis of many diseases such as hepatic injury, kidney diseases, *Helicobacter pylori* infection and halitosis [5–9]. As reported, the concentration of ammonia in human exhaled breath is approximately in the range of 50 parts per billion (ppb) to 5 parts per million (ppm) [4]. In order to improve previous medical testing methods, there is an urgency to design an ultra-low concentration ammonia sensor. According to the operating mechanism of gas sensors, there are mainly two kinds of gas detection technology, namely, spectrum analysis and gas sensor systems [10–13]. The gas sensor system technology is suitable for online and timely

detection, while, spectrum analysis methods such as spectrometry and chromatography have a long and complicated analysis cycle [10].

Different materials are under study by different research groups for gas sensor applications. The most widely sensitive materials for gas sensors are the metal oxide materials, including ZnO, SnO₂, NiO, and so on [14–16]. These metal oxide semiconductors usually have very excellent gas sensing properties. Additionally, metal hydroxides [17], metal sulfides [14], binary metal oxides [18], and other materials have been extensively and studied as sensitive materials, and usually have better gas sensing properties.

Graphene and its derivatives are considered as promising gas sensor materials in the field of ultra-high sensitivity detection because of their high surface area and high carrier mobility [19–23]. Research aimed at improving the gas sensing properties of graphene to detect the ultra-low concentration ammonia gas is an emerging field. Graphene is functionalized with metal oxides (such as SnO₂, ZnO, Cu₂O, WO₃) to form hybrid nanostructures sensors [24–29], because the high surface area of graphene may cause synergetic effects in achieving a good gas response at room temperature while blended with metal oxides, especially due to formation of a p-n junctions, and the resulting novel sensors may exhibit better performance than those of the individual materials [29]. Graphene has functionalized by decoration with metal nanoparticles (NPs) (including AuNPs, AgNPs) for gas sensing [30–35]. The sensitivity depends on the degree of coverage of the metal NPs on the graphene [35]. Su et al. have prepared an ammonia sensor with Pd/SnO₂/RGO ternary composite, the ammonia gas sensitivity of which reached 25 ppm [36]. An ammonia gas sensor prepared by RGO and P3TH, also could detect 10 ppm concentrations of ammonia [37]. Both of them have used as gas sensing material modified RGO as the adsorption layer with RGO as the conductive sensing material whose conductivity is far less than that of graphene. However, the sensitivity of the above sensors does not reach ultra-low detection concentrations.

The electron transport of graphene is highly sensitive to most gas molecules owing to its high mobility and presence of a large number of surface atoms in its 2D structure [38–40]. The devices based on graphene are expected to have relatively low Johnson noise and 1/f noise because of their high conductance and low crystal defect density, respectively [39,41]. However, graphene is intrinsically rather inert owing to its few gas molecule adsorption sites [42]. On the other hand, RGO has inherent chemical defects, and attached functional groups which can provide a large number of adsorption sites beneficial to adsorbing ammonia gas, but the conductivity is much worse compared to that of graphene, meanwhile, Johnson noise and 1/f noise of RGO are higher than that of pristine graphene.

This paper proposes a new RGO-Gr hybrid structure based on pristine CVD graphene decorated with RGO to combine the advantages of both graphene and RGO, in order to obtain good gas sensitivity and low noise characteristics. The effects of different RGO reduction time on gas sensing properties have also been studied.

2. Materials and Methods

2.1. Preparation of Graphene and RGO

Graphene was synthesized on copper foil (#13382, 99.8%, Alfa Aesar, Haverhill, MA, USA) by a chemical vapor deposition (CVD) method [43]. RGO was prepared by a multiple steps process. Initially, GO (30 mg, #XF002-1, XF Nano Inc., Nanjing, China) was dispersed in deionized water (40 mL) and sonicated for 4 h. Next, after adjusting the pH value of the solution by adding 25% ammonia solution (140 µL), 80% hydrazine hydrate (20 µL) was added as a reducing agent to the solution which was sonicated for 3 min. Then, the solution was transferred into a reaction kettle and heated to 90 °C using the water bath for different reduction times to get different samples. Finally, the obtained solution was centrifuged and washed with deionized water several times and the final product was obtained. The final samples were labeled as RGO0 (GO), RGO10, RGO20 and RGO40,

corresponding to the samples prepared using different reduction times (0, 10, 20 and 40 min). For more clarification, the synthesis process of RGO is schematically described in Figure 1.

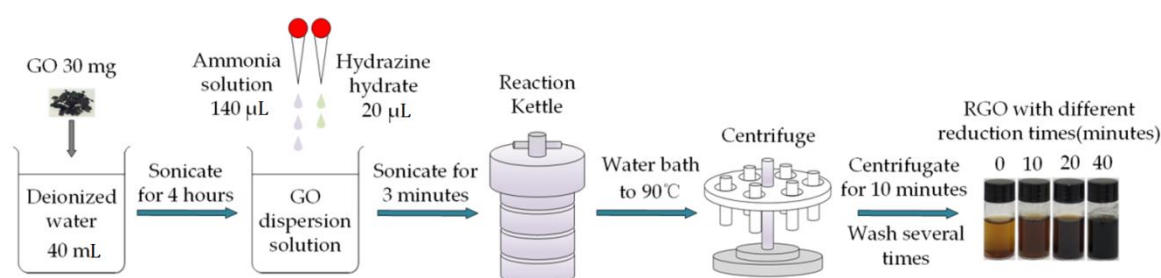


Figure 1. Synthesis flowchart of RGO with four different reduction times.

2.2. Fabrication of RGO-Gr Hybrids Gas Sensor

The fabrication process of the RGO-Gr hybrid gas sensors is shown in Figure 2. Firstly, the RGO solution was evenly spin coated on the surface of CVD graphene on copper foil, which was placed on a heating table and dried for 5 min at 50 °C. Secondly, the copper foil was etched away with prepared ammonium persulfate. Thirdly, the RGO-Gr hybrid film was obtained and washed several times in deionized water. Finally, RGO-Gr hybrid was transferred to a fresh interdigital electrode (IDE) and the RGO-Gr hybrid gas sensor device was thus obtained. The graphene on the IDEs was used as the conductive layer while RGO decorated on graphene was used as the ammonia molecule adsorption layer.

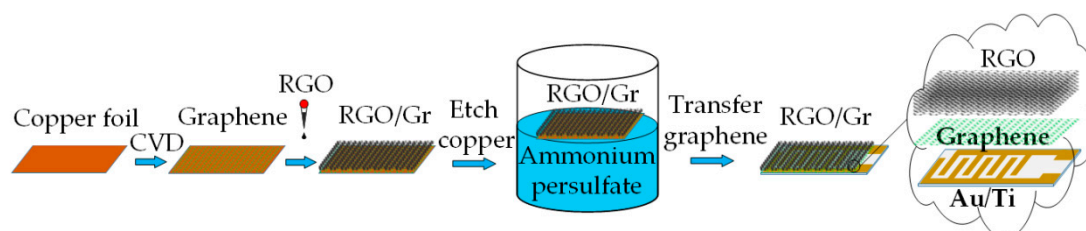


Figure 2. Fabrication process of the RGO-Gr hybrid gas sensors.

In this graphene transfer process, RGO replaced PMMA (polymethyl methacrylate) as the protective layer of graphene, which not only avoided the organic contamination caused by the introduction of PMMA, but also reduced the damage to the graphene by reducing the experimental steps. Six sensors have been made to conduct comparative research. The sensing materials of the first two sensors were pristine CVD graphene and pristine RGO (RGO0), namely Sensor-1 and Sensor-2, respectively. The sensing materials of the latter four sensors were all RGO-Gr hybrids structures with four different reduction times of RGO. The six sensors could be classified into three kinds as listed in Table 1.

Table 1. Relationship of sensor name and sensing material.

Sensors	Sensor-1	Sensor-2	Sensor-3-1	Sensor-3-2	Sensor-3-3	Sensor-3-4
Materials	Graphene	RGO0	RGO0-Gr	RGO10-Gr	RGO20-Gr	RGO40-Gr

2.3. Material Characterization

The morphology and structure of the graphene were characterized with a scanning electron microscope (SEM, S-4800, Hitachi, Tokyo, Japan). The graphene transferred to the IDEs was measured at room temperature with a Raman spectrometer (JY HR800, Horiba, Lille, France) at 514 nm with

an output power of 20 mW. X-ray photoelectron spectroscopy (XPS) (Axis Ultra DLD, Kratos Inc., Manchester, UK) was used to determine the elemental composition and state of the composites.

2.4. Gas Sensing Detection

Ammonia gas detection experiments were carried out in a simple homemade testing chamber, while the total volume of chamber, drying tube and filling pipe was measured and calculated as 4.67 L as shown in Figure 3. The drying pipe filled with potassium hydroxide as a desiccant was used to convert injected ammonia solution into dry ammonia gas which was passed into the chamber by an air pump (MEDOVP0125-V1005-P2-1411, Nitto Kohki, Tokyo, Japan). Details of the calibration and control of ammonia concentration and humidity are provided in the electronic Supporting Information (SI). The sensor temperature and the relative humidity (RH) in the test chamber were room temperature (about $25\text{ }^{\circ}\text{C} \pm 2\text{ }^{\circ}\text{C}$) and $30 \pm 4\%$, respectively. The resistances of proposed gas sensors were detected and recorded by a multimeter (2000, Keithley Instruments, Cleveland, OH, USA) and a computer running the Lab-VIEW software for automatic data storage under different ammonia concentration conditions. The concentrations of ammonia gas were varied from 0.5 to 50 ppm.

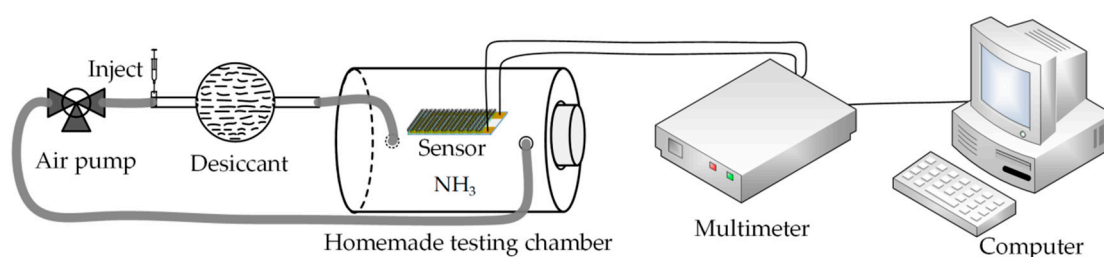


Figure 3. Schematic diagram of the gas sensing system.

3. Results and Discussion

3.1. Characterization of the Morphology and Structure of Materials

Figure 4a illustrates schematic diagram of the RGO-Gr hybrid sensor. Graphene on the IDEs is used as the conductive layer, and RGO decorated on the graphene is used as gas adsorption layer, which forms the hybrid structure of the sensor. Figure 4b shows a SEM image of CVD grown graphene on an IDE. The CVD graphene is flat and smooth, as shown in Figure 4c. To know the quality of the as-prepared graphene, Raman spectroscopy examinations were conducted on different places. The intensity of the D band of graphene is so small that it can almost be ignored, which means that the graphene is of very good quality with little impurities and defects. The intensity ratio (I_{2D}/I_G) of as synthesized graphene is 1.61, which implies that the as prepared graphene is monolayer [44]. A SEM image of RGO0 is shown in Figure 4d. The Raman spectrum of RGO0 from the inset in Figure 4d shows that the intensity of the D band of RGO0 has increased sharply compared to graphene, which means that RGO0 contains a lot of defects.

XPS measurements have been executed on RGO0, RGO10, RGO20 and RGO40 to study the functional group changes depending on the RGO reduction time. Figure 5 shows the contents of various groups in the four RGOs with different reduction time (a, b, c and d correspond to RGO0, RGO10, RGO20 and RGO40, respectively). The relative intensity of each element as a function of binding energy is shown in Figure 5. The Gaussian fitted peaks around binding energy of 284.8, 286.5, 287.8 and 289.2 eV show the existence of carbon sp^2 (C-C), hydroxyl (C-OH), epoxy (C-O-C) and carboxyl (COOH) functional groups in the as-synthesized RGO-Gr hybrid samples, respectively [45]. These XPS results show the surface of RGO has a mixed composition of C-C, C-OH, C-O-C and COOH. The total percentage of the three groups (C-OH, C-O-C and COOH) decreased with the RGO reduction time, and the percentage of C-OH is always the highest among the three groups, then C-O-C, and COOH is the lowest.

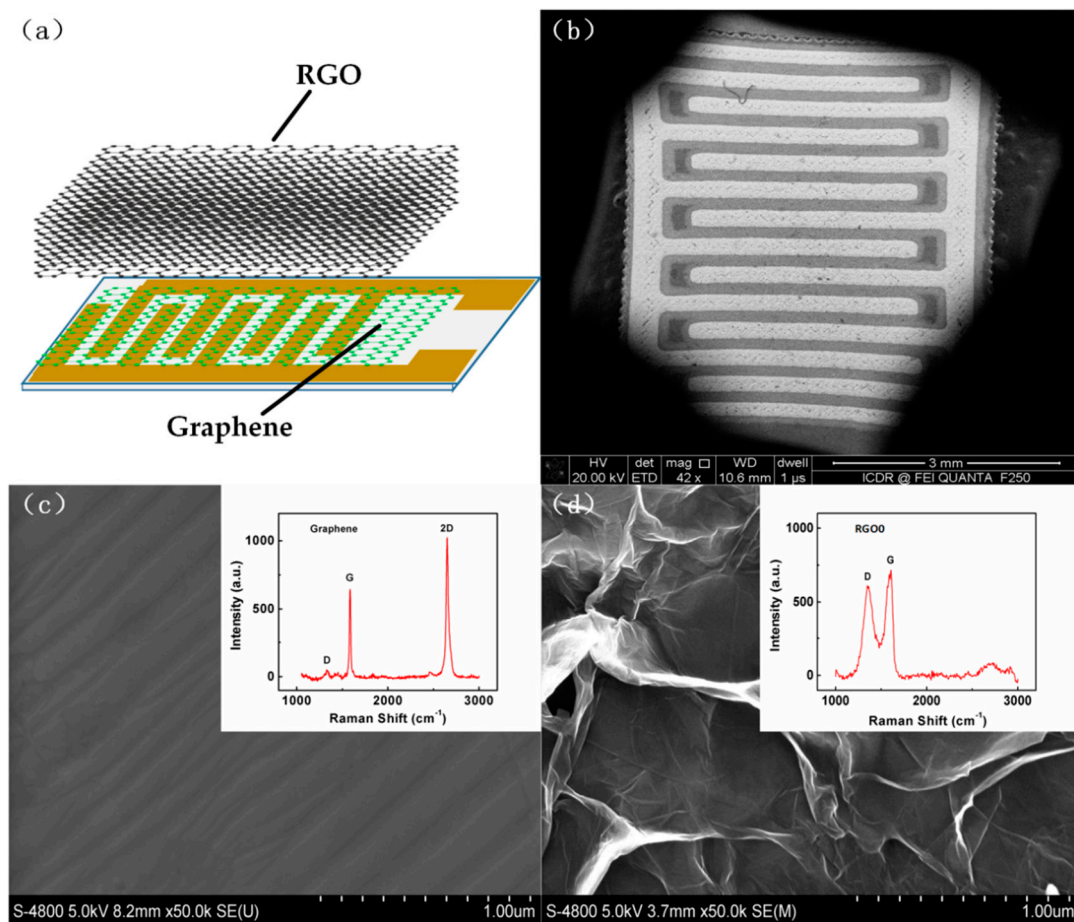


Figure 4. (a) Schematic diagram of RGO-Gr hybrids gas sensors; (b) SEM image of CVD Graphene on IDE electrode; SEM image and Raman spectra of the (c) graphene and (d) RGO.

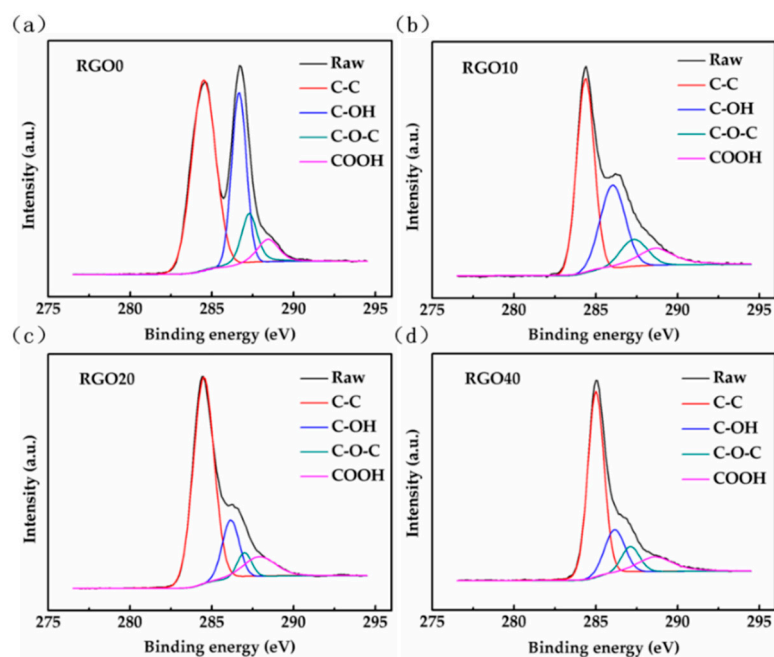


Figure 5. XPS spectra of Gaussian fitted peaks of (a) RGO0; (b) RGO10; (c) RGO20; and (d) RGO40, respectively.

Meanwhile, the total percentage of the three groups (C-OH, C-O-C and COOH) in RGO10 is much more than those in the latter two RGOs (RGO20 and RGO40). The protocol and fitting results of split peak are shown in the SI. When the reduction time reaches 40 min, the reduction of RGO is almost complete. As the reduction time continues to increase, the percentages of each functional group will tend to be nearly stable.

3.2. Sensing Mechanism of Hybrid Structure Sensor

The exposure of three sorts of sensors to ammonia gas (NH₃) results in an increment in the electrical resistance ratio (Figure 6a).

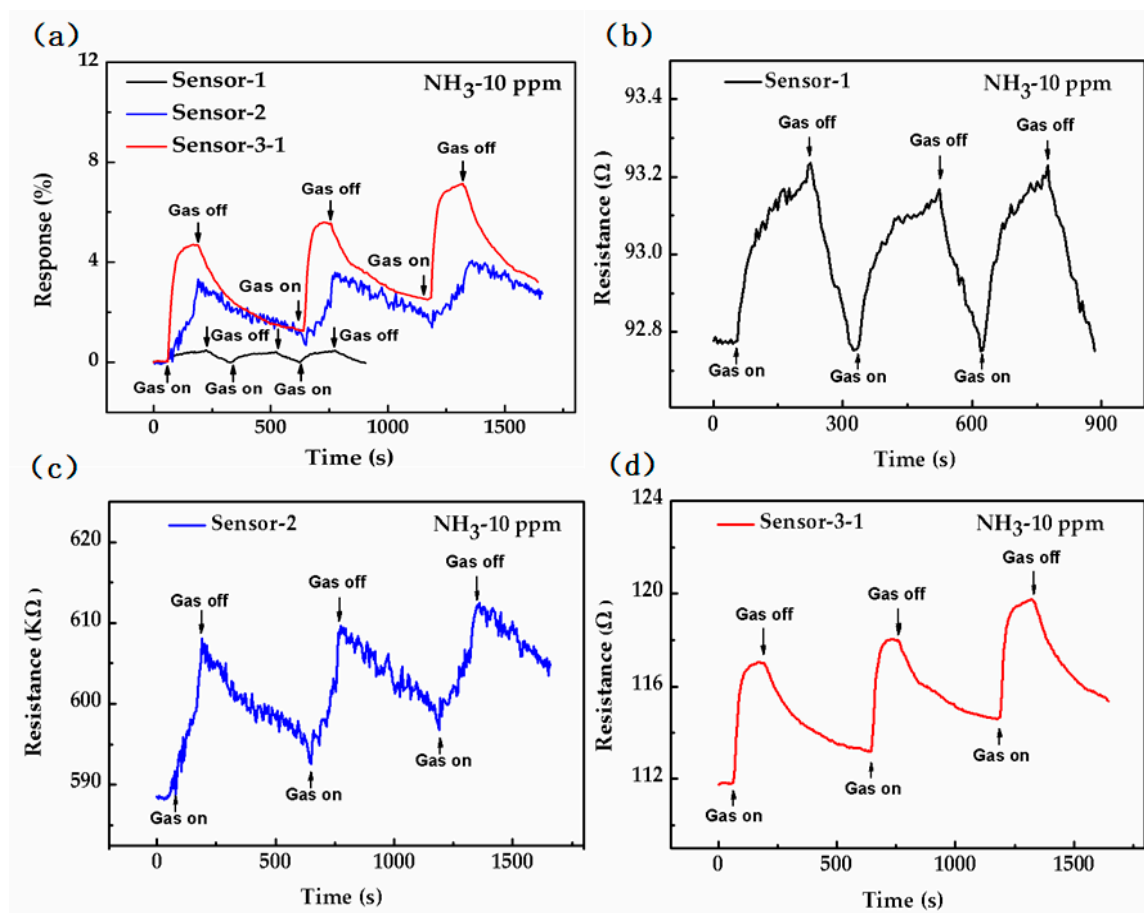


Figure 6. (a) Response of three types of sensors to 10 ppm ammonia; Resistance changes of (b) Sensor-1; (c) Sensor-2; and (d) Sensor-3-1 to 10 ppm ammonia gas respectively

R_{ammonia} and R_{air} are the electrical resistance values with and without ammonia gas, respectively. Electrical resistance response is defined as a ratio expressed in percentage:

$$\text{Response}(\%) = \frac{R_{\text{ammonia}} - R_{\text{air}}}{R_{\text{air}}} \times 100\% \quad (1)$$

The black, blue and red curves correspond to Sensor-1, Sensor-2 and Sensor-3-1, respectively. The resistances of the sensors increase dramatically when exposed to 10 ppm ammonia gas, and then drop with the ammonia gas off (i.e., air on). According to Figure 6a, Sensor-1 gives a negligible electrical resistance ratio resistance increment reading when exposed to NH₃ (0.48%) in comparison to Sensor-2 (3.32%) and Sensor-3-1 (4.7%), as shown in the Table 2. This clearly suggests a high response of Sensor-3-1 towards NH₃. A plausible sensing mechanism was established. CVD graphene is a p-type material with holes as major carriers under ambient conditions originating from adsorbed water

or oxygen molecules [46]. The resistance of the sensor rises in the ammonia because the recombination of electrons produced by ammonia molecule adsorption and holes in graphene, which leads to a decrease of the carrier concentration in graphene. The exposure of the three sorts of sensors to continuous NH_3 cycles has demonstrated good consistency and reversibility (Figure 6).

Table 2. Sensing materials and electrical parameters comparison of three sensors.

Sensor Name	Sensor-1	Sensor-2	Sensor-3-1
Materials	Graphene	RGO0	RGO0-Gr
Resistance of sensor	92.78 Ω	588 k Ω	111.7 Ω
Response	0.48%	3.32%	4.7%
SNR	87	22	304

Although graphene has the lowest resistance ($\sim 92.78 \Omega$) as seen in Figure 6b, its gas sensing properties are not very good because of the lack of gas adsorption sites in its perfect lattice structure. Compared to Sensor-1 with graphene only, Sensor-2 with RGO0 only has higher resistance ($\sim 588 \text{ k}\Omega$) as seen in Figure 6c. In contrast RGO0 has introduced a large number of adsorption sites including defects and functional groups (as shown in Figure 5a) that greatly increases the amount of gas adsorption and transferred charges in the ammonia gas as seen in Figure 6c, which causes a dramatic increase in the gas sensing response. Unfortunately, Sensor-2 with RGO0 has also introduced noise because of its low signal-to-noise ratio (SNR, calculated as shown in Equation (2) [47]) of 22 and 5.36 k Ω resistance variation (Figure 6c) which is caused by $1/f$ noise and Johnson noise. The $1/f$ noise mainly results from the changes of minority carrier number and carrier mobility caused by defects in a sensing material such as graphene [39]. Johnson noise originates from the irregular thermal motion of the carrier, and is proportional to the impedance of the sensing material [41]. The reason why Sensor-2 has obvious increase in noise is that both of its large amount of defects and high resistance ($\sim 588 \text{ k}\Omega$) lead to a tremendous increase in $1/f$ noise and Johnson noise. On the contrary, Sensor-1 has a high SNR of 87 because of its fewer defects and low resistance ($\sim 92.78 \Omega$) from the complete lattice structure of CVD graphene.

It is well known that the gas sensitivity characteristics of sensors are mainly related to the conductivity and adsorption sites of their sensing materials [48]. The response of Sensor-3-1 (red line) is better than that of the other two because it combines the advantages of both graphene and RGO. The graphene is used as the conductive layer and electron acceptor, and electron transfer between homogenous materials is easier due to RGO0 being an electron donor and a derivative of graphene. Simultaneously, the adsorption layer of RGO0 can provide abundant adsorption sites because of its large number of functional groups and defects. Therefore, the gas sensitivity of Sensor-3-1 is the best among the three sensors as shown in Figure 6a. The noise problems of RGO0 were not observed in Sensor-3-1, because the graphene and RGO0 combined with a large region of π - π bonds, defects and functional groups in RGO0 that do not affect the graphene conductive layer. Sensor-3-1 is a hybrid structure of graphene and RGO0 and its equivalent resistance is equal to the sum of the parallel resistance values of graphene and RGO. The resistance of Sensor-3-1 ($\sim 111.7 \Omega$) is very close to that of Sensor-1 ($\sim 92.78 \Omega$), which is much less than 588 k Ω of Sensor-2. As a result, the noise introduced by Sensor-3-1 is very close to that of Sensor-1, such as the resistance variation caused by noise (0.09 Ω of Sensor-3-1 to 0.054 Ω of Sensor-1). Thus, Sensor-3-1 has very low noise because its resistance is very low close to that of CVD graphene. Sensor-3-1 has produced a SNR of 304 as shown in Figure 6d which is not only much higher than that of Sensor-2 (~ 22), but also higher than that of Sensor-1 (~ 87), because the gas sensing response of Sensor-3-1 is much higher compared to Sensor-1.

The recovery characteristics of Sensor-1 are faster than those of the other two sensors, because gas adsorption of graphene is a physisorption phenomenon with a weak binding energy, while the gas adsorption of RGO0 is a chemisorption phenomenon with strong binding energy.

The SNR could be obtained according to reference [47]. The signal power is derived from the resistance variation (ΔR) during gas introduction. The power of noise is electrical noise from instrumentation before gas introduction. In this case, the electrical noise is determined by the root-mean-square ($\text{rms}_{\text{noise}}$) value of the initial resistance (i.e., before gas introduction). The SNR could be obtained after resistance variation is divided by $\text{rms}_{\text{noise}}$ as follows:

$$\text{SNR} = \frac{\Delta R}{\text{rms}_{\text{noise}}} \quad (2)$$

3.3. Effect of the RGO Reduction Time on Sensing Performance

To study the influence of the hybrid structure on the response, comparative gas sensing experiments have been conducted on Sensor-3-1, Sensor-3-2, Sensor-3-3 and Sensor-3-4. Figure 7 shows the gas sensing response of the four sensors under seven different concentrations of ammonia (0.5, 1, 2.5, 5, 10, 25, 50 ppm). The profiles of the four sensors are similar, in which the gas sensing response gradually increases with the gas concentration. As it can be seen clearly, the response of Sensors-3-1 exhibits the least value, Sensors-3-3 with a RGO20 on graphene structure shows higher NH_3 variation value than Sensors-3-4 with RGO40, while Sensors-3-2 with a RGO10 on graphene structure exhibits the highest response compared to the other three sensors.

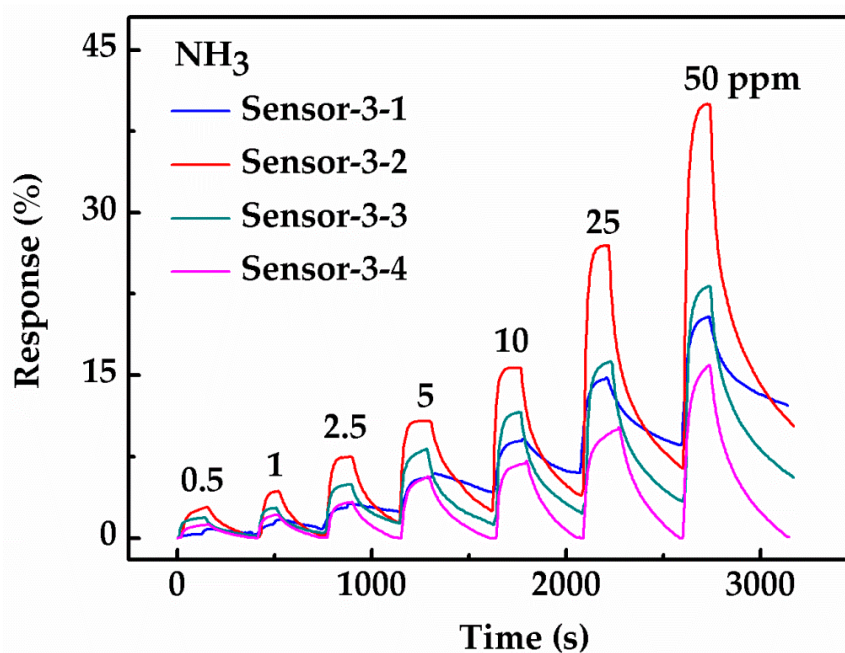


Figure 7. Gas sensing response of four hybrid sensors under seven different ammonia concentrations (0.5, 1, 2.5, 5, 10, 25, 50 ppm).

In order to study the effects of different RGO reduction times on the hybrid structure gas sensors, the comparative response-time profiles of the four sensors are plotted in Figure 8a with a gas on (150 s)/gas off (350 s) cycle of 500 s at 10 ppm ammonia. The gas sensing response of Sensor-3-2 is the best, and the sensing response of Sensor-3-4 is more than that of Sensor-3-1, but less than that of Sensor-3-3. With the increase of RGO reduction time, the gas sensing response of the sensors increases firstly and then decreases, reaching the highest value in Sensor-3-2 (10 min of reduction time).

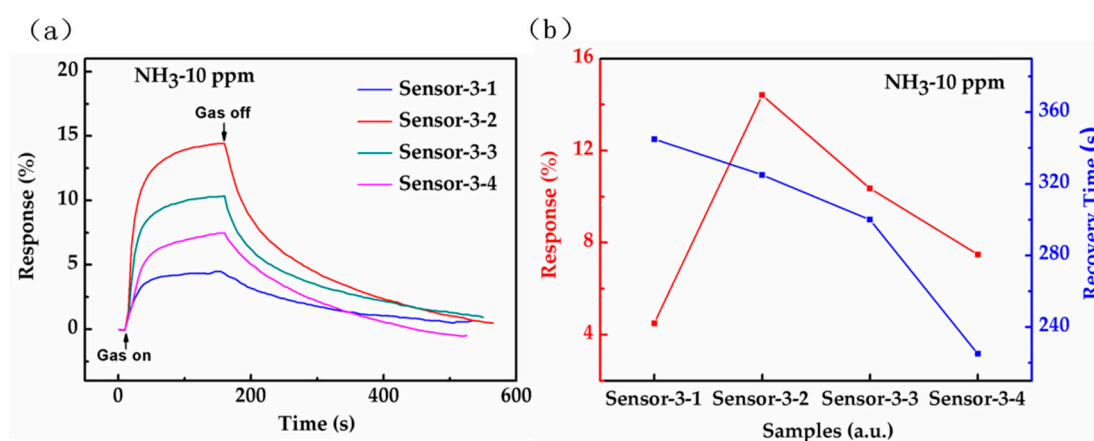


Figure 8. (a) Gas sensing response curves of four sensors to 10 ppm ammonia; (b) Gas sensing and recovery time of four sensors for 10 ppm ammonia.

For one thing, RGO mainly contains three kinds of functional groups (C-OH, C-O-C and COOH), respectively. Graphene modified with each group individually constitutes a particular hybrid structure. This experiment has compared the values of current and sensitivity of three hybrid structures during ammonia molecule adsorption, as described in the SI. The conclusion can be drawn that the hybrid structure of graphene modified with C-OH outputs the highest current and sensitivity compared to the other two hybrid structures. Therefore, this experiment has extracted the ratio of C-OH and C-C groups in the Gaussian fitted peaks of the sensors Sensor-3-1, Sensor-3-2, Sensor-3-3, and Sensor-3-4, as shown in the following Table 3. Except for RGO0, the C-OH group ratio of Sensor-3-2 is the highest among the other three RGO on graphene hybrid structures, so it has the highest response to ammonia gas, as shown in Figure 8.

Table 3. Structural and electrical parameters comparison of the RGO-Gr hybrid gas sensors.

Sensor Name	Sensor-3-1	Sensor-3-2	Sensor-3-3	Sensor-3-4
Adsorption layer/Resistance	RGO0/588 k Ω	RGO10/18.77 k Ω	RGO20/5.34 k Ω	RGO40/1.62 k Ω
Hybrid Resistance	111.7 Ω	176 Ω	167 Ω	191 Ω
C-OH/C-C	0.82	0.62	0.34	0.27
Response	4.7%	14.67%	10.49%	6.43%
SNR	304	1008	720	517

From Figure 5 and Table 3, Sensor-3-1 shows the highest C-OH group ratio and least response among the four sensors. RGO0 is rich in various functional groups and this results in a high resistance of ~588 k Ω . On the contrary, the amount of functional groups of the other three RGOs is less than that of RGO0 and this results in low resistances of less than 20 k Ω [46,49].

The interaction between ammonia molecules and C-OH causes a change of the resistance of the adsorbent layer, which also affects the resistance of the graphene transport layer via π - π stacking. The coupling efficiency in the hybrid structure is obviously reduced because of the high resistance of RGO0, which can counteract the advantages of a higher C-OH ratio, and attenuate the response of the sensor. Although the C-OH ratio of RGO0 is higher than that of the other three RGOs, the excessive adsorption resistance of RGO0 counteracts the transmission current of the hybrid structure. Therefore, in general, the responses of the other three RGO-Gr hybrid structures are higher than that of the RGO0-Gr hybrid structure, and Sensor-3-2 is the best among the four sensors. Due to the best gas sensing response and the use of graphene as a conductive layer without introducing additional noise, the signal-to-noise ratio of Sensor-3-2 is the highest, up to 1008.

The response and recovery times, a significant indicator for gas sensors, are defined as the time to reach 90% of the final highest value after the gas is injected and the time to reach 10% of the highest value after the gas is removed, respectively [46]. The profile shows that the response times of four sensors are very close, and are all less than 1 min. The recovery times in Figure 8b of Sensor-3-1, Sensor-3-2, Sensor-3-3, Sensor-3-4 to NH₃ are 345 s, 325 s, 300 s and 225 s, respectively. This means that the recovery time decreases monotonically as the RGO reduction time increases.

As an almost insulator, RGO0 has a particularly poor conductivity. However, with the increase of the reduction time, the functional groups in the RGO gradually decrease, which leads to the increase in the conductivity of RGO and the recovery speed of sensors. Therefore, the recovery time decreases monotonically with RGO reduction time.

The exposure of the four RGO-Gr hybrid gas sensors to three continuous cycles of three different concentrations of ammonia is shown in Figure 9a. As the concentration of ammonia increases, the gas sensing response increases. Meanwhile, the results perfectly match that the gas sensing response of RGO on graphene hybrid that increases first and then decreases with the increase of the RGO reduction time. All four sensors have demonstrated good consistency and reversibility under three kinds of ammonia concentration (10, 25, 50 ppm).

As for Figure 9b, RGO on graphene hybrids structure give a negligible response when exposed to organic vapours such as ethanol, formaldehyde and isopropanol compared to 10 ppm NH₃. This clearly suggests the strong selectivity of the RGO on graphene hybrid structure towards NH₃. The strong selectivity towards NH₃ may be due to the strong reducing and donor behaviour of NH₃ among the introduced vapours, as this paper shows that NH₃ has injected a much higher amount of negative charge carriers into the RGO on graphene hybrids compared to other introduced vapours. Therefore, the negative charge carrier density of the RGO on graphene hybrids is greatly enhanced.

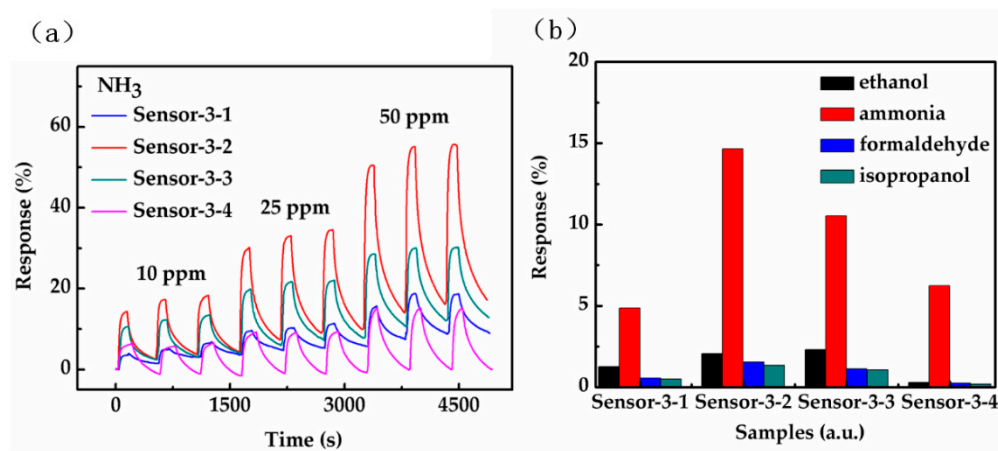


Figure 9. (a) Profile of four RGO-Gr hybrids gas sensors after three continuous cycles under three different concentrations of ammonia; (b) selectivity response when exposed to ethanol, formaldehyde, isopropanol and ammonia at 10 ppm.

In order to obtain the detection limit of these gas sensors to ammonia, Sensor-3-2 is selected as the reference sensor for the detection limit due to its excellent gas sensing response under all concentrations as compared to the other sensors. The linear responses with increase of NH₃ concentration of Sensor-3-2 at seven ammonia concentrations are illustrated separately in Figure 7. Data at low concentration has been extracted in order to investigate the minimum concentration detection limit of Sensor-3-2. A straight fitting line is shown in Figure 10a. The detection limit is calculated using Equation (3) [27], and the details are given in the SI:

$$DL(\text{ppb}) = 3 \frac{\text{rms}_{\text{noise}}}{\text{slope}} = 36 \text{ ppb}, \quad (3)$$

where, $\text{rms}_{\text{noise}}$ is the root-mean-square deviation of sensor noise, and the calculated value of $\text{rms}_{\text{noise}}$ is 0.019. slope is the slope of the black line (1.55 in Figure 10a). Finally, the gas detection limit of Sensor-3-2 is calculated to be 36 ppb.

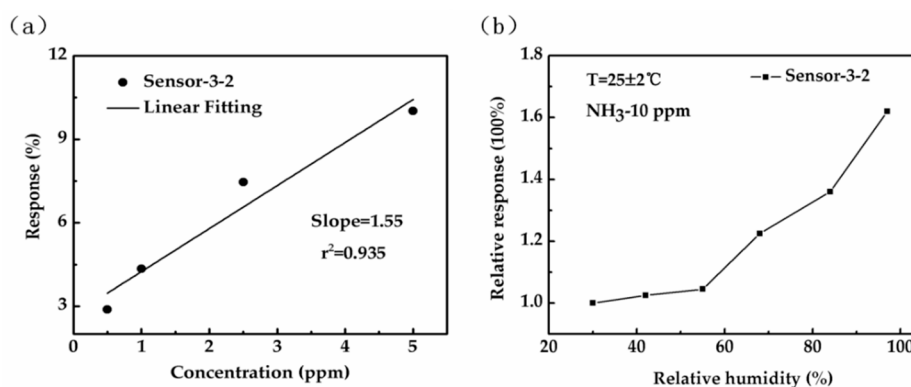


Figure 10. (a) Linear response with increase of ammonia concentration of Sensor-3-2; (b) relative response of Sensor-3-2 to 10 ppm ammonia under different relative humidity values.

Because humidity is an important factor affecting the gas sensitivity of graphene sensors, the effect of humidity on the gas sensing properties of the graphene sensors was studied. Here, the response of Sensor-3-2 toward 10 ppm ammonia gas under different humidity conditions was tested, as shown in Figure 10b. The abscissa represents the change of relative humidity, and the ordinate represents the multiple of the gas sensing response of Sensor-3-2 under different relative humidity in response to 10 ppm ammonia. It can be seen from the profile that when the relative humidity is at a low level, the gas sensing response change of Sensor-3-2 is relatively small, while when the relative humidity reaches 68%, the gas sensing response of the sensor is enhanced significantly with the increase of relative humidity. This is due to the emergence of ammonium hydroxide (NH_4OH) derived from ammonia molecules and water molecules on graphene, which has stronger N doping ability than ammonia, so the gas sensing response of the graphene-based sensors increases evidently [50].

The performance of our sensor was compared with several sensors recently reported by other groups. Table 4 summarizes the sensing materials, gas concentration, response and operating temperature of these studies. The first three articles mainly used polymers and their complexes with other nanomaterials as gas-sensitive materials [51–53]. Although it is possible to work at room temperature, the sensitivities of these sensors are not very high. SnO_2 modified with Pt nanoparticles has a good gas-sensitive response [54], however, a high operating temperature limits its application. Interestingly, our RGO-Gr hybrids film had the best gas sensitivity among these devices at room temperature.

Table 4. Comparison of various indicators between different ammonia sensors.

Sensing Materials	Gas Concentration	Response	Operating Temperature	Reference
Graphene/PANI	20 ppm	3.65%	25 °C	[51]
Polyaniline	5 ppm	0.25%	25 °C	[52]
PANI/ SnO_2	10 ppm	5%	25 °C	[53]
Pt/ SnO_2	50 ppm	25%	115 °C	[54]
RGO/Graphene	0.5 ppm	2.88%	25 °C	This Work

4. Conclusions

In summary, a hybrid structure gas sensor of reduced GO decorated graphene (RGO-Gr) has been designed to take advantages of both the high conductivity of graphene with its perfect lattice structure and RGO with lots of adsorption sites to realize ultra-low concentration ammonia

detection. The RGO-Gr hybrid sensor not only exhibits the best gas sensing performance compared to pristine graphene or pristine RGO sensors, but also greatly improves the anti-noise ability with the SNR increasing from 22 to 1008 compared to the RGO gas sensor. In order to further improve the properties of these gas sensors, the influence of RGO reduction time on sensing properties has been investigated. The RGO10-Gr hybrid structure exhibits an excellent response of 2.88% at 0.5 ppm and good selectivity to ammonia gas in contrast to ethanol, formaldehyde and isopropanol. The gas detection limit of the RGO10-Gr hybrid structure is calculated to be 36 ppb. We believe that this work may be valuable for the future research on gas sensors.

Supplementary Materials: The following are available online at <http://www.mdpi.com/1424-8220/18/9/3147/s1>, Figure S1: Device geometry models of graphene. (a) Pure graphene. Graphene decorated with (b) epoxy (C–O–C), (c) a hydroxyl (C–OH) and (d) carboxyl (–COOH) groups for ammonia sensing, Figure S2: (a) I–V curves and (b) the normalized I–V curves for NH₃ adsorption on pure graphene, graphene decorated with an epoxy (C–O–C), a hydroxyl (C–OH), and carboxyl (–COOH), respectively.

Author Contributions: C.W. designed the study project and experiments, collected and analyzed the data, and wrote the paper. S.L. provided guidance on the experiments. X.L. provided funds and guidance on research ideas, analyzed the data, and revised the paper. S.G. and P.C. simulated the experiments with software. X.W., W.L. and H.L. helped and gave advice on the experiments.

Funding: This research was funded by the Science and Technology Planning Project of Guangdong Province, National Natural Science Foundation of China, Shaanxi Natural Science Foundation, Science and Technology Planning Project of Zhejiang Province and grant number No. 2017A010103004, 91123018, 51625504, 61671368, 2014JM7277 and 2017C31087, respectively.

Acknowledgments: This work was financially supported by grants from Science and Technology Planning Project of Guangdong Province, China (2017A010103004) and the National Natural Science Foundation of China (No. 91123018, 51625504, 61671368), Shaanxi Natural Science Foundation (2014JM7277), Science and Technology Planning Project of Zhejiang Province, China (2017C31087). Some XPS work was done at International Center for Dielectric Research (ICDR), Xi'an Jiaotong University, Xi'an, China; Authors also thank Dai and Yang for their help in using XPS.

Conflicts of Interest: The authors declare that there is no conflict of interests regarding the publication of this study.

References

1. Patil, U.V.; Ramgir, N.S.; Karmakar, N.; Bhogale, A.; Debnath, A.K.; Aswal, D.K.; Gupta, S.K.; Kothari, D.C. Room temperature ammonia sensor based on copper nanoparticle intercalated polyaniline nanocomposite thin films. *Appl. Surf. Sci.* **2015**, *339*, 69–74. [[CrossRef](#)]
2. Wu, B.; Zhang, X.F.; Huang, B.J.; Zhao, Y.T.; Cheng, C.T.; Chen, H.D. High-Performance Wireless Ammonia Gas Sensors Based on Reduced Graphene Oxide and Nano-Silver Ink Hybrid Material Loaded on a Patch Antenna. *Sensors* **2017**, *17*, 2070. [[CrossRef](#)] [[PubMed](#)]
3. Solga, S.F.; Mudalel, M.L.; Spacek, L.A.; Risby, T.H. Fast and accurate exhaled breath ammonia measurement. *J. Vis. Exp.* **2014**, *88*, e51658. [[CrossRef](#)] [[PubMed](#)]
4. Aguilar, A.D.; Forzani, E.S.; Nagahara, L.A.; Amlani, I.; Tsui, R.; Tao, N.J. A breath ammonia sensor based on conducting polymer nanojunctions. *IEEE Sens. J.* **2008**, *8*, 269–273. [[CrossRef](#)]
5. Dai, M.Z.; Lin, Y.L.; Lin, H.C.; Zan, H.W.; Chang, K.T.; Meng, H.F.; Liao, J.W.; Tsai, M.J.; Cheng, H. Highly Sensitive Ammonia Sensor with Organic Vertical Nanojunctions for Noninvasive Detection of Hepatic Injury. *Anal. Chem.* **2013**, *85*, 3110–3117. [[CrossRef](#)] [[PubMed](#)]
6. Spacek, L.A.; Mudalel, M.; Tittel, F.; Risby, T.H.; Solga, S.F. Clinical utility of breath ammonia for evaluation of ammonia physiology in healthy and cirrhotic adults. *J. Breath Res.* **2015**, *9*, 047109. [[CrossRef](#)] [[PubMed](#)]
7. Hibbard, T.; Crowley, K.; Kelly, F.; Ward, F.; Holian, J.; Watson, A.; Killard, A.J. Point of Care Monitoring of Hemodialysis Patients with a Breath Ammonia Measurement Device Based on Printed Polyaniline Nanoparticle Sensors. *Anal. Chem.* **2013**, *85*, 12158–12165. [[CrossRef](#)] [[PubMed](#)]
8. Güntner, A.T.; Righettoni, M.; Pratsinis, S.E. Selective sensing of NH₃ by Si-doped α -MoO₃ for breath analysis. *Sens. Actuators B Chem.* **2016**, *223*, 266–273. [[CrossRef](#)]

9. Ogimoto, Y.; Selyanchyn, R.; Takahara, N.; Wakamatsu, S.; Lee, S.W. Detection of ammonia in human breath using quartz crystal microbalance sensors with functionalized mesoporous SiO₂ nanoparticle films. *Sens. Actuators B Chem.* **2015**, *215*, 428–436. [[CrossRef](#)]
10. Janata, J.; Josowicz, M. Organic semiconductors in potentiometric gas sensors. *J. Solid State Electrochem.* **2009**, *13*, 41–49. [[CrossRef](#)]
11. Agbor, N.E.; Cresswell, J.P.; Petty, M.C.; Monkman, A.P. An optical gas sensor based on polyaniline Langmuir-Blodgett films. *Sens. Actuators B Chem.* **1997**, *41*, 137–141. [[CrossRef](#)]
12. Nagai, T.; Tamura, S.; Imanaka, N. Solid Electrolyte Type NH₃ Gas Sensor Applicable in a Humid Atmosphere. *Electrochemistry* **2010**, *78*, 126–128. [[CrossRef](#)]
13. Lee, Y.C.; Huang, H.; Tan, O.K.; Tse, M.S. Semiconductor gas sensor based on Pd-doped SnO₂ nanorod thin films. *Sens. Actuators B Chem.* **2008**, *132*, 239–242. [[CrossRef](#)]
14. Zhang, J.; Liu, X.H.; Neri, G.; Pinna, N. Nanostructured Materials for Room-Temperature Gas Sensors. *Adv. Mater.* **2016**, *28*, 795–831. [[CrossRef](#)] [[PubMed](#)]
15. Wang, Y.R.; Liu, B.; Xiao, S.H.; Wang, X.H.; Sun, L.M.; Li, H.; Xie, W.Y.; Li, Q.H.; Zhang, Q.; Wang, T.H. Low-Temperature H₂S Detection with Hierarchical Cr-Doped WO₃ Microspheres. *ACS Appl. Mater. Interfaces* **2016**, *8*, 9674–9683. [[CrossRef](#)] [[PubMed](#)]
16. Joshi, N.; Hayasaka, T.; Liu, Y.M.; Liu, H.L.; Oliveira, O.N.; Lin, L.W. A review on chemiresistive room temperature gas sensors based on metal oxide nanostructures, graphene and 2D transition metal dichalcogenides. *Microchim. Acta* **2018**, *185*, 213. [[CrossRef](#)] [[PubMed](#)]
17. Liu, X.H.; Ma, T.T.; Pinna, N.; Zhang, J. Two-Dimensional Nanostructured Materials for Gas Sensing. *Adv. Funct. Mater.* **2017**, *27*, 1702168. [[CrossRef](#)]
18. Joshi, N.; da Silva, L.F.; Jadhav, H.S.; Shimizu, F.M.; Suman, P.H.; M'Peko, J.C.; Orlandi, M.O.; Seo, J.G.; Mastelaro, V.R.; Oliveira, O.N. Yolk-shelled ZnCo₂O₄ microspheres: Surface properties and gas sensing application. *Sens. Actuators B-Chem.* **2018**, *257*, 906–915. [[CrossRef](#)]
19. Gautam, M.; Jayatissa, A.H. Gas sensing properties of graphene synthesized by chemical vapor deposition. *Mater. Sci. Eng. C* **2011**, *31*, 1405–1411. [[CrossRef](#)]
20. Lu, G.H.; Ocola, L.E.; Chen, J.H. Reduced graphene oxide for room-temperature gas sensors. *Nanotechnology* **2009**, *20*, 445502. [[CrossRef](#)] [[PubMed](#)]
21. Fowler, J.D.; Allen, M.J.; Tung, V.C.; Yang, Y.; Kaner, R.B.; Weiller, B.H. Practical Chemical Sensors from Chemically Derived Graphene. *ACS Nano* **2009**, *3*, 301–306. [[CrossRef](#)] [[PubMed](#)]
22. Basu, S.; Bhattacharyya, P. Recent developments on graphene and graphene oxide based solid state gas sensors. *Sens. Actuators B Chem.* **2012**, *173*, 1–21. [[CrossRef](#)]
23. Toda, K.; Furue, R.; Hayami, S. Recent progress in applications of graphene oxide for gas sensing: A review. *Anal. Chim. Acta* **2015**, *878*, 43–53. [[CrossRef](#)] [[PubMed](#)]
24. Zhang, H.; Feng, J.C.; Fei, T.; Liu, S.; Zhang, T. SnO₂ nanoparticles-reduced graphene oxide nanocomposites for NO₂ sensing at low operating temperature. *Sens. Actuators B Chem.* **2014**, *190*, 472–478. [[CrossRef](#)]
25. Liu, S.; Yu, B.; Zhang, H.; Fei, T.; Zhang, T. Enhancing NO₂ gas sensing performances at room temperature based on reduced graphene oxide-ZnO nanoparticles hybrids. *Sens. Actuators B Chem.* **2014**, *202*, 272–278. [[CrossRef](#)]
26. Zhou, L.; Shen, F.; Tian, X.; Wang, D.; Zhang, T.; Chen, W. Stable Cu₂O nanocrystals grown on functionalized graphene sheets and room temperature H₂S gas sensing with ultrahigh sensitivity. *Nanoscale* **2012**, *5*, 1564–1569. [[CrossRef](#)] [[PubMed](#)]
27. Srivastava, S.; Jain, K.; Singh, V.N.; Singh, S.; Vijayan, N.; Dilawar, N.; Gupta, G.; Senguttuvan, T.D. Faster response of NO₂ sensing in graphene-WO₃ nanocomposites. *Nanotechnology* **2012**, *23*, 205501. [[CrossRef](#)] [[PubMed](#)]
28. An, X.Q.; Yu, J.C.; Wang, Y.; Hu, Y.M.; Yu, X.L.; Zhang, G.J. WO₃ nanorods/graphene nanocomposites for high-efficiency visible-light-driven photocatalysis and NO₂ gas sensing. *J. Mater. Chem.* **2012**, *22*, 8525–8531. [[CrossRef](#)]
29. Chatterjee, S.G.; Chatterjee, S.; Ray, A.K.; Chakraborty, A.K. Graphene-metal oxide nanohybrids for toxic gas sensor: A review. *Sens. Actuators B Chem.* **2015**, *221*, 1170–1181. [[CrossRef](#)]
30. Cui, S.M.; Mao, S.; Wen, Z.H.; Chang, J.B.; Zhang, Y.; Chen, J.H. Controllable synthesis of silver nanoparticle-decorated reduced graphene oxide hybrids for ammonia detection. *Analyst* **2013**, *138*, 2877–2882. [[CrossRef](#)] [[PubMed](#)]

31. Si, Y.C.; Samulski, E.T. Exfoliated Graphene Separated by Platinum Nanoparticles. *Chem. Mater.* **2008**, *20*, 6792–6797. [[CrossRef](#)]
32. Hong, W.J.; Bai, H.; Xu, Y.X.; Yao, Z.Y.; Gu, Z.Z.; Shi, G.Q. Preparation of Gold Nanoparticle/Graphene Composites with Controlled Weight Contents and Their Application in Biosensors. *J. Phys. Chem. C* **2010**, *114*, 1822–1826. [[CrossRef](#)]
33. Lu, L.M.; Li, H.B.; Qu, F.L.; Zhang, X.B.; Shen, G.L.; Yu, R.Q. In situ synthesis of palladium nanoparticle-graphene nanohybrids and their application in nonenzymatic glucose biosensors. *Biosens. Bioelectron.* **2011**, *26*, 3500–3504. [[CrossRef](#)] [[PubMed](#)]
34. Zanjani, S.M.M.; Sadeghi, M.M.; Holt, M.; Chowdhury, S.F.; Tao, L.; Akinwande, D. Enhanced sensitivity of graphene ammonia gas sensors using molecular doping. *Appl. Phys. Lett.* **2016**, *108*, 666.
35. Song, H.; Li, X.; Cui, P.; Guo, S.X.; Liu, W.H.; Wang, X.L. Morphology optimization of CVD graphene decorated with Ag nanoparticles as ammonia sensor. *Sens. Actuators B Chem.* **2017**, *244*, 124–130. [[CrossRef](#)]
36. Su, P.G.; Yang, L.Y. NH₃ gas sensor based on Pd/SnO₂/RGO ternary composite operated at room-temperature. *Sens. Actuators B Chem.* **2016**, *223*, 202–208. [[CrossRef](#)]
37. Ye, Z.; Jiang, Y.; Tai, H.; Yuan, Z. The investigation of reduced graphene oxide/P3HT composite films for ammonia detection. *Integr. Ferroelectr.* **2014**, *154*, 73–81. [[CrossRef](#)]
38. Hu, N.T.; Yang, Z.; Wang, Y.Y.; Zhang, L.L.; Wang, Y.; Huang, X.L.; Wei, H.; Wei, L.M.; Zhang, Y.F. Ultrafast and sensitive room temperature NH₃ gas sensors based on chemically reduced graphene oxide. *Nanotechnology* **2014**, *25*, 025502. [[CrossRef](#)] [[PubMed](#)]
39. Schedin, F.; Geim, A.K.; Morozov, S.V.; Hill, E.W.; Blake, P.; Katsnelson, M.I.; Novoselov, K.S. Detection of individual gas molecules adsorbed on graphene. *Nat. Mater.* **2007**, *6*, 652–655. [[CrossRef](#)] [[PubMed](#)]
40. Ghosh, R.; Singh, A.; Santra, S.; Ray, S.K.; Chandra, A.; Guha, P.K. Highly sensitive large-area multi-layered graphene-based flexible ammonia sensor. *Sens. Actuators B Chem.* **2014**, *205*, 67–73. [[CrossRef](#)]
41. Zhou, Y.; Jiang, Y.D.; Xie, T.; Tai, H.L.; Xie, G.Z. A novel sensing mechanism for resistive gas sensors based on layered reduced graphene oxide thin films at room temperature. *Sens. Actuators B Chem.* **2014**, *203*, 135–142. [[CrossRef](#)]
42. Zhou, Y.; Lin, X.G.; Huang, Y.K.; Guo, Y.C.; Gao, C.; Xie, G.Z.; Jiang, Y.D. Impact of further thermal reduction on few-layer reduced graphene oxide film and its n-p transition for gas sensing. *Sens. Actuators B Chem.* **2016**, *235*, 241–250. [[CrossRef](#)]
43. Li, X.; Shi, J.J.; Pang, J.C.; Liu, W.H.; Liu, H.Z.; Wang, X.L. Graphene Channel Liquid Container Field Effect Transistor as pH Sensor. *J. Nanomater.* **2014**, *2014*, 233. [[CrossRef](#)]
44. Kahng, Y.H.; Lee, S.; Choe, M.; Jo, G.; Park, W.; Yoon, J.; Hong, W.K.; Cho, C.H.; Lee, B.H.; Lee, T. A study of graphene films synthesized on nickel substrates: Existence and origin of small-base-area peaks. *Nanotechnology* **2010**, *22*, 45706–45709. [[CrossRef](#)] [[PubMed](#)]
45. Robinson, J.T.; Perkins, F.K.; Snow, E.S.; Wei, Z.Q.; Sheehan, P.E. Reduced Graphene Oxide Molecular Sensors. *Nano Lett.* **2008**, *8*, 3137–3140. [[CrossRef](#)] [[PubMed](#)]
46. Bai, S.L.; Zhao, Y.B.; Sun, J.H.; Tian, Y.; Luo, R.X.; Li, D.Q.; Chen, A.F. Ultrasensitive room temperature NH₃ sensor based on a graphene-polyaniline hybrid loaded on PET thin film. *Chem. Commun.* **2015**, *51*, 7524–7527. [[CrossRef](#)] [[PubMed](#)]
47. Kim, H.Y.; Lee, K.; McEvoy, N.; Yim, C.; Duesberg, G.S. Chemically Modulated Graphene Diodes. *Nano Lett.* **2013**, *13*, 2182–2188. [[CrossRef](#)] [[PubMed](#)]
48. Zhang, L.S.; Wang, W.D.; Liang, X.Q.; Chu, W.S.; Song, W.G.; Wang, W.; Wu, Z.Y. Characterization of partially reduced graphene oxide as room temperature sensor for H₂. *Nanoscale* **2011**, *3*, 2458–2460. [[CrossRef](#)] [[PubMed](#)]
49. Novoselov, K.S.; Geim, A.K.; Morozov, S.V.; Jiang, D.; Zhang, Y.; Dubonos, S.V.; Grigorieva, I.V.; Firsov, A.A. Electric field effect in atomically thin carbon films. *Science* **2004**, *306*, 666–669. [[CrossRef](#)] [[PubMed](#)]
50. Song, H.; Lei, S.; Li, X.; Guo, S.; Cui, P.; Wei, X.; Liu, W.; Liu, H. Quantitative description of Ag nanoparticles-graphene hybrids with optimized morphology on sensing performance. *Sens. Actuators A Phys.* **2017**, *271*. [[CrossRef](#)]
51. Wu, Z.Q.; Chen, X.D.; Zhu, S.B.; Zhou, Z.W.; Yao, Y.; Quan, W.; Liu, B. Enhanced sensitivity of ammonia sensor using graphene/polyaniline nanocomposite. *Sens. Actuators B Chem.* **2013**, *178*, 485–493. [[CrossRef](#)]
52. Kumar, L.; Rawal, I.; Kaur, A.; Annapoorni, S. Flexible room temperature ammonia sensor based on polyaniline. *Sens. Actuators B Chem.* **2017**, *240*, 408–416. [[CrossRef](#)]

53. Bai, S.L.; Tian, Y.L.; Cui, M.; Sun, J.H.; Tian, Y.; Luo, R.X.; Chen, A.F.; Li, D.Q. Polyaniline@SnO₂ heterojunction loading on flexible PET thin film for detection of NH₃ at room temperature. *Sens. Actuators B-Chem.* **2016**, *226*, 540–547. [[CrossRef](#)]
54. Liu, X.; Chen, N.; Han, B.Q.; Xiao, X.C.; Chen, G.; Djerdj, I.; Wang, Y.D. Nanoparticle cluster gas sensor: Pt activated SnO₂ nanoparticles for NH₃ detection with ultrahigh sensitivity. *Nanoscale* **2015**, *7*, 14872–14880. [[CrossRef](#)] [[PubMed](#)]



© 2018 by the authors. Licensee MDPI, Basel, Switzerland. This article is an open access article distributed under the terms and conditions of the Creative Commons Attribution (CC BY) license (<http://creativecommons.org/licenses/by/4.0/>).